Chemical Science

ROYAL SOCIETY OF CHEMISTRY

EDGE ARTICLE

View Article Online
View Journal | View Issue

Cite this: *Chem. Sci.*, 2024, **15**, 10436

All publication charges for this article have been paid for by the Royal Society of Chemistry

Received 29th February 2024
Accepted 24th May 2024

DOI: 10.1039/d4sc01432d

rsc.li/chemical-science

A high-performance triboelectric nanogenerator with dual nanostructure for remote control of switching circuit†

Yanhong Dong,[ac] Yange Feng*[ab] and Daoai Wang *[abc]

Preparing nanostructured surfaces has been considered an effective method to improve the output of triboelectric nanogenerators (TENGs), but how to quickly prepare materials with a nanostructured surface for TENGs has always been a challenge. Here, polypropylene nanowires and electrospun nylon 11 nanofibers were successfully prepared through a simple and time-saving method with a high success rate. Compared with a flat TENG, the output performance of a dual nanostructured TENG is enhanced by more than 5 times. After 1*H*,1*H*,2*H*,2*H*-perfluorooctyl trichlorosilane was assembled on the surface of the polypropylene film, the dual nanostructured TENG achieved the maximum output with the short-circuit current, output voltage, and charge density of 63.3 μA, 1135 V and 161.5 μC m^{-2}, respectively. Compared with a planar structured TENG, the short-circuit current and output voltage were enhanced by about 18 times, and the charge density was increased by about 36 times. In addition, the TENG showed good working stability with almost no decrease in output after continuous operation for 193 000 cycles. The electricity generated by this TENG can successfully light up 1280 LEDs and continuously power a multi-functional electronic watch. Finally, the triboelectric signal generated by this TENG was used to control an optocoupler switch, indicating good application prospects in a remote control switching circuit.

Introduction

Recently, triboelectric nanogenerators (TENGs) based on the coupling effect of triboelectricity and electrostatic induction have attracted widespread attention due to their advantages such as light weight, diverse materials, easy fabrication, and low cost.[1–3] TENGs have been proven to be an effective low-frequency harvesting technology that can convert various types of mechanical energy, such as human movement,[4,5] wind energy,[6–9] and water energy,[10–12] into electrical energy. The electric energy generated by a triboelectric generator is used for the power supply of electronic equipment,[13,14] as a pressure sensor,[15,16] for motion monitoring,[17–19] health monitoring,[20–24] environmental monitoring,[25–27] air or water purification,[28,29] showing very good application prospects.

To improve the applications of the triboelectric nanogenerators, researchers have proposed various methods to improve their output. A common method to improve the output of a triboelectric generator is to micro-nano-process the friction layer material to increase the contact area and thereby increase the amount of generated triboelectric charge.[30,31] In addition, the generation of tribocharges can be improved by chemically modifying the frictional material surface to increase the triboelectric polarity gap between the two friction layer materials.[32–36] Relying solely on nanotechnological treatment of the material surface or chemical modification of the surface of the material has made limited improvements to the performance of TENGs. Therefore, micro-nano processing is combined with chemical surface modification of the materials to effectively improve the output of the triboelectric nanogenerators.[37] At present, the friction layer of a triboelectric generator is composed mainly of two plane films or a plane film and structured film. If both friction layers of the triboelectric generator can be made into nanostructures, the effective contact area may be further increased to improve the output. Current methods for micro-nano treatment of triboelectric material surfaces include inductively coupled plasma etching, template replication, and chemical etching.[38–42] These methods can achieve micro-nano processing of some polymer materials such as PTFE, PI, PDMS and other materials. However, they also face some problems, such as inductively coupled plasma etching, which is less effective at processing thermoplastic materials and whose equipment is more

[a]*State Key Laboratory of Solid Lubrication, Lanzhou Institute of Chemical Physics, Chinese Academy of Sciences, Lanzhou 730000, China. E-mail: fengyange@licp.cas.cn; wangda@licp.cas.cn*

[b]*Shandong Laboratory of Advanced Materials and Green Manufacturing at Yantai, Yantai 265503, China*

[c]*Qingdao Center of Resource Chemistry and New Materials, Qingdao 266104, China*

† Electronic supplementary information (ESI) available. See DOI: https://doi.org/10.1039/d4sc01432d

expensive. There have been studies using anodic aluminum oxide (AAO) templates to obtain regular polypropylene nanowires through hot pressing, which can effectively improve the output of the triboelectric nanogenerators.[43] However, the production process of an AAO template is cumbersome, cycle is long, cost is high, and film removal success rate is low, which limits its application. Therefore, it is very necessary to develop a simple and rapid method for preparing polymer nanowires that can be used in conjunction with surface chemical modification methods to improve the output of the triboelectric generators.

Herein, polypropylene (PP) nanowires with regular nanostructure were successfully prepared by a hot pressing method. Instead of AAO templates, a polycarbonate (PC) membrane is chosen as the template mainly because it is low in cost, easy to obtain, and has many aperture specifications. The most important thing is that the AAO template takes a long time to demold and generates a lot of heat, which reduces the success rate of demolding. Due to the characteristics of polypropylene being insoluble in chloroform and polycarbonate being soluble in chloroform, putting the hot-pressed mixed film into chloroform for about 30 seconds can completely remove the PC template, which greatly reduces the mold removal time and increases the success rate of mold removal. Assembling a polypropylene nanowire film and nylon (NY) nanofiber film into a dual nanostructure TENG can effectively improve the output of the triboelectric nanogenerator. Compared with flat PP and flat NY, its output is increased by more than 5 times. In addition, 1*H*,1*H*,2*H*,2*H*-perfluorooctyltrichlorosilane (PFTS) was successfully assembled on the surface of the polypropylene film using a vapor deposition method to further enhance the output of the triboelectric nanogenerator. Compared with a planar structure TENG, the short-circuit current (I_{sc}) and output voltage (V_o) of the PFTS-enhanced dual nanostructure TENG were increased by about 18 times. The electricity generated by this TENG can successfully light up 1280 LEDs in real time and continuously supply power to a multi-functional electronic watch with a temperature measurement function, proving good application prospects in micro power supply devices. In addition, the nanowire film based TENG was integrated into a printed circuit board (PCB) circuit to control the 'on' and 'off' of an optocoupler switch, indicating good application prospects in intelligent switch control.

Experimental

Materials

Polypropylene film (industrial grade, 50 μm), polycarbonate membrane (pore sizes 200 μm and 400 μm, Whatman, UK), 1*H*,1*H*,2*H*,2*H*-perfluorooctyltrichlorosilane (PFTS, 98%, Sigma-Aldrich), nylon 11 (NY11, pellets, 3 mm, $M = 201.31$ g mol^{-1}, Sigma-Aldrich) were used as received. An Ag target was purchased from ZhongNuo Advanced Material (Beijing) Technology Co., Ltd. Other solvents were purchased from Tianjin Chemical Reagents Corp. and used without further purification.

Fabrication of PP nanowire array

PP nanowire array friction layers were prepared by a simplified hot processing technique using a porous polycarbonate membrane as the template. Typically, a flat PP film with a thickness of 50 μm and a polycarbonate membrane with different pore sizes were placed in the middle of two glass plates and later moved to an oven at 200 °C by applying a load of 2 N cm^{-2} on the top glass plate. After maintaining the temperature at 200 °C for about 1 h and cooling down without releasing the load, the prepared PP nanowire-polycarbonate composite was put into chloroform for 1 min to remove the PC template. Last, after dissolving the polycarbonate template, PP nanowire arrays with different pore size were obtained.

Fluoropolymer modification of PP nanowires

To modify PP films with 1*H*,1*H*,2*H*,2*H*-perfluorooctyltrichlorosilane, oxygen plasma treated PP substrates with flat or nanowire structures were put in a sealed container by dropping 10 μL of PFTS and placed on a hot plate at 80 °C for 2 h. Then, prepared samples were transferred to an oven at 120 °C to fully assemble PFTS to obtain final PP-PFTS nanowires.

Preparation of nylon 11 film and nanowires

Initially, 2 g of nylon 11 was mixed with 8.6 g of formic acid and 9.4 g of dichloromethane in a 50 mL triangular flask and later stirred for 1 h to make sure all the nylon had dissolved. The prepared solution was left to stand for one day to allow the whole solution to reach a uniform state. In the first step, a 200 nm thick Ag layer was plated on a piece of 4.5 cm × 4.5 cm sized kapton film through ion sputtering. Then, an Ag conductive adhesive was used to fasten the Cu lead onto the Ag layer. The NY solution was spin-coated on the Ag surface with a rotation speed of 2000 rpm for 60 s and dried in an oven at 80 °C for 2 h to remove residual solvents. The NY solution was loaded into a syringe where the distance between the needle and collector was 20 cm. To prepare NY nanofibers, electrospinning was conducted at 15 kV with a feed rate of NY solution of 0.5 mL h^{-1} and dried in an oven at 80 °C for 2 h to remove the residual solvents.

Preparation of PP and NY based TENGs

PP and NY friction pairs were assembled into a triboelectric generator with a dual nanowire structure. First, the flat PP or PP nanowire film was cut into 4.5 cm × 4.5 cm size. A 200 nm thick Ag layer was plated on the reverse side of the PP films through ion sputtering. Then, a copper wire was fixed on the surface of the Ag film with copper foil tape and silver conductive glue. Then, the PP and NY friction pairs were assembled into a triboelectric generator with two flexible PI supports to enable it to automatically restore after pressing.

Characterization

The surface morphologies of PP and NY were characterized with a JEOL JSM-6710F field emission scanning electron microscope (FE-SEM, Japan Electron Optics Laboratory) and Zeiss EVO 10

scanning electron microscope. The surface composition was characterized by X-ray photoelectron spectroscopy (XPS, ESCALAB 250xi) and an energy dispersive spectrometer (EDS, Oxford Xplore 15). The contact angle (CA) was tested with a DSA-100 optical contact angle meter (Kruss Company, Ltd., Germany) at ambient temperature (25 °C). A commercial linear mechanical motor was used to drive prepared TENGs under 5 Hz contact frequency. When an external force was imposed on the TENG by a linear motor, triboelectric charges were generated between the two different friction layers, resulting in a triboelectric potential and electric output in the external circuit. The output voltage was measured using an MDO32 oscilloscope (Tektronix, America), while the short-circuit current was measured using an SR570 low-noise current amplifier (Stanford Research System, America). The surface potentials of PP, PFTS-PP and nylon films were measured with a Kelvin probe force microscope (KPFM, Multimode 8, Bruker, Germany) with a conductive probe (EFM, NanoSensors, Switzerland). All density functional theory (DFT) calculations were carried out with Gaussian G16W with the B3LYP-D3BJ method and 6-311g (d, p) basis set. Orbital composition and electrostatic surface potential analysis were realized by Multiwfn.[44,45] The electrostatic surface potential, HOMO and LUMO maps were drawn with Visual Molecular Dynamics (VMD).[46]

Results and discussion

The PP nanowire array friction layers were prepared by a simplified hot processing technique using a porous polycarbonate membrane as a template, as shown in Fig. 1a. PFTS was successfully assembled on the PP nanowire surface *via* a vapor deposition method. Nylon nanofibers were fabricated by electrospinning, as shown in Fig. 1b. Details of all experiments can be found in the Experimental section. The PP and NY friction pairs with a size of 4.5 cm × 4.5 cm were assembled into a triboelectric generator with a dual nanowire structure, as shown in Fig. 1c.

Similar to most contact-separation mode triboelectric nanogenerators (CS-TENGs), the working principle of a PP@NY triboelectric nanogenerator is based on the coupling effect of triboelectrification and induction electrification. The working mechanism of a PP-NY based TENG is illustrated in Fig. 2. As shown in Fig. 2a, before PP contacts NY, no charge transfer occurs. When the PP and NY layers are pressed to contact, positive charges are generated on NY, and negative charges are generated on the PP surface (Fig. 2b). Due to the electrostatic induction effect, the Ag conducting layer generates opposite charges to the PP friction layer, resulting in the formation of a current flow from the NY electrode to the PP electrode during the release process (Fig. 2c). Once the charges reach the balanced state, no current flows in the circuit (Fig. 2d). Similarly, during the pressing process, a reverse current is detected from the PP electrode to the NY electrode (Fig. 2e). Thus, by coupling the contact electrification with electrostatic induction effects, alternating electricity is generated while the TENG experiences a contact-separation process.

Fig. 3a–c shows the surface morphology SEM images and cross-sectional SEM image of the PP nanowires fabricated through a PC template with a 400 nm pore size. According to the images, uniform nanowires were successfully fabricated with about 470 ± 45 nm diameter and 8.9 μm length. Fig. 3d–f shows the surface morphology SEM images and cross-sectional SEM image of the PP nanowires fabricated through a PC template with a 200 nm pore size. According to the images, the uniform nanowires were successfully fabricated with about 209 ± 25 nm diameter and 8.3 μm length. To facilitate data comparison, we abbreviate the above two PP nanowires to 400 PP and 200 PP, respectively. Fig. 3g–i shows the surface morphology SEM images and cross-sectional SEM image of the NY nanofibers fabricated through electrospinning. It can be seen from figures that the nylon nanofibers are very uniform with about 426 ± 121 nm diameter. The thickness of the nylon nanofibers film is about 17.5 μm, according to Fig. 3i. The statistical results of the diameters of the polypropylene nanowires and nylon nanofibers can be seen in Fig. S2.†

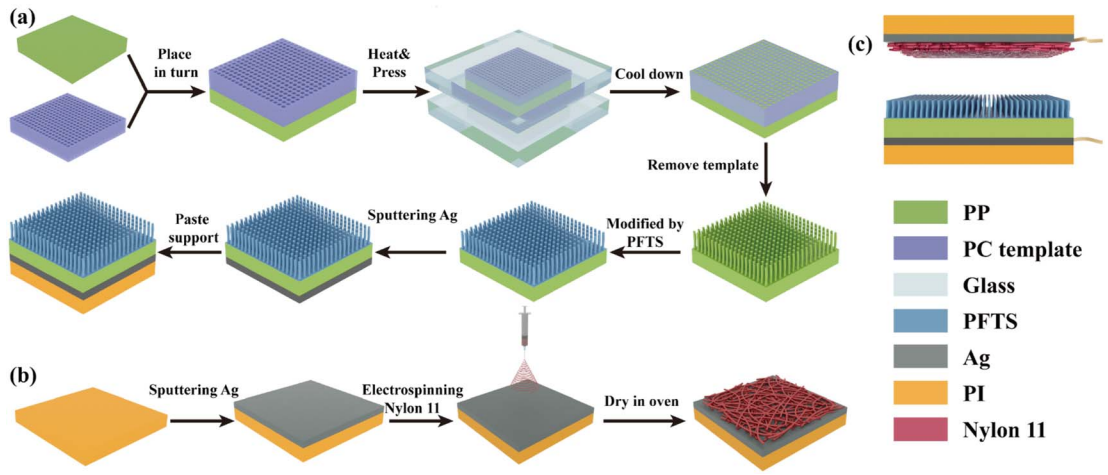

Fig. 1 Schematic image of the fabrication process of (a) a PFTS-modified PP nanowire array based triboelectric electrode and (b) a nylon nanowire based triboelectric electrode; (c) schematic image of a TENG composed of PP nanowires and nylon nanofibers.

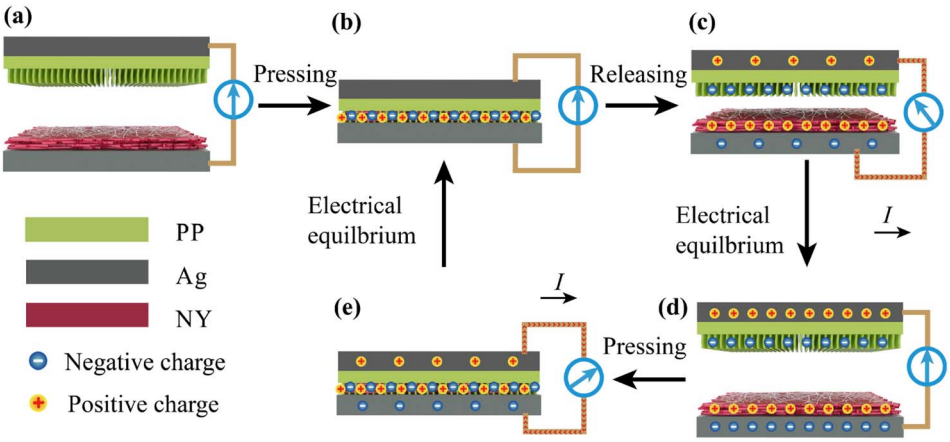

Fig. 2 Scheme of the working mechanism and charge generation process: (a) original separation state, (b) pressed into contact to generate frictional charges, (c) released to generate induced charges, current flows from the NY part to the PP part, (d) reaching the electrical balance state when no current flows in the external circuit, (e) pressed into contact again, when current flows from the PP part to the NY part.

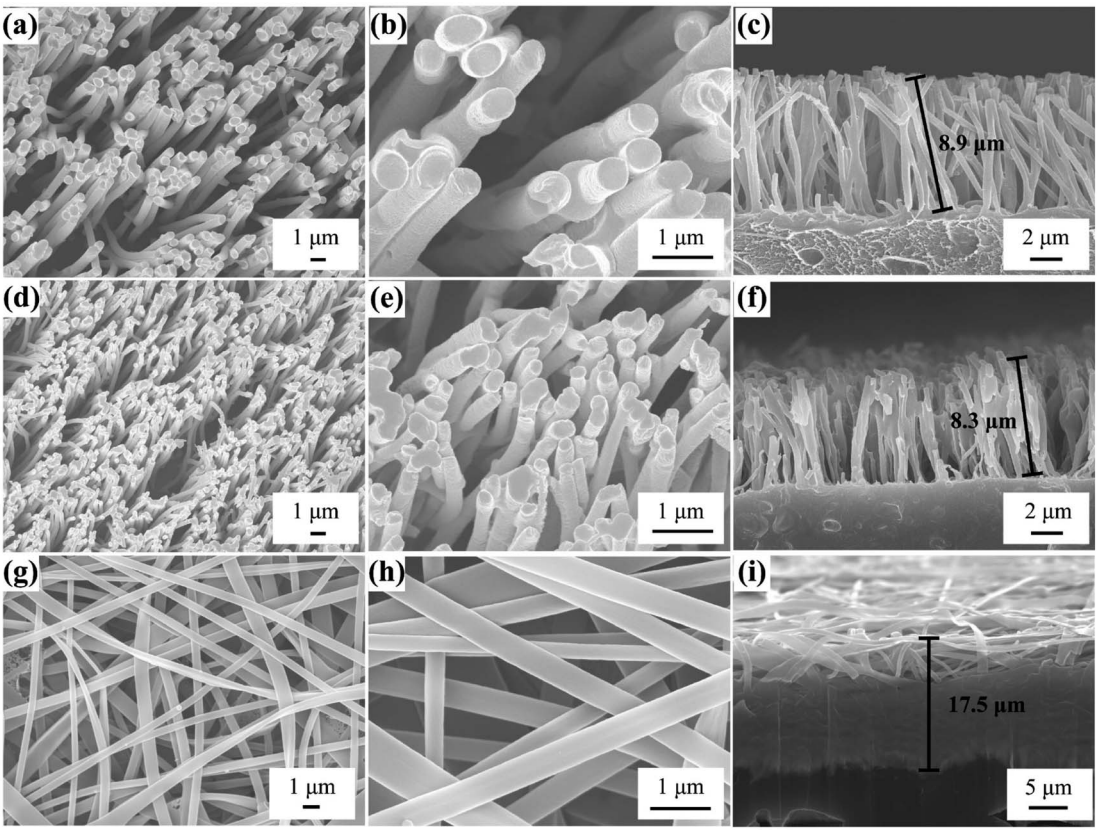

Fig. 3 (a–c) Surface morphology and cross-sectional SEM images of 400 PP nanowires; (d–f) surface morphology and cross-sectional SEM images of 200 PP nanowires; and (g–i) surface morphology and cross-sectional SEM images of NY nanofibers.

To study the effect of nanostructure on the output of a triboelectric nanogenerator, friction layer materials with a planar structure and nanowire structure were combined, as shown in Fig. 4a–d. This combination includes main four different groups: flat PP@flat NY, PP nanowire@flat NY, flat PP@NY nanowire and PP nanowire@NY nanowire. Since there are two types of the polypropylene nanowire, 200 PP and 400 PP, a total of six triboelectric nanogenerator outputs with different friction layer materials were tested, and the short-circuit current (I_{sc}), output voltage (V_o) and charge density results are shown in Fig. 4e–g. According to the results, I_{sc}, V_o and charge density follow the same trend: that is, the output of the planar structured TENG is smaller than that of the nanostructured TENG. It was demonstrated that nanostructures can increase the contact

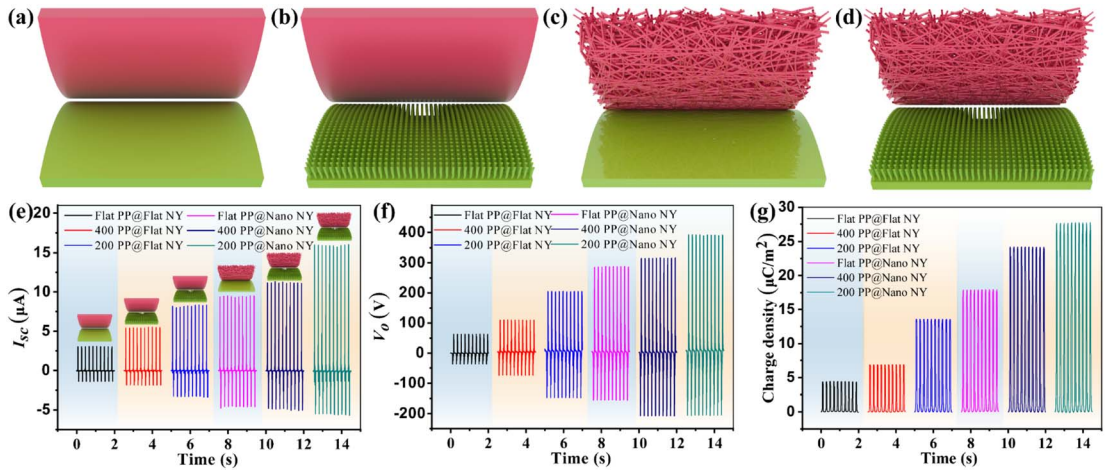

Fig. 4 Schematic images of TENGs composed of (a) flat PP and flat NY, (b) PP nanowires and flat NY, (c) flat PP and NY nanofibers, (d) PP nanowires and NY nanofibers and the output performances of TENGs composed of flat PP, PP nanowires, flat NY and NY nanofibers: (e) I_{sc}, (f) V_o and (g) charge density.

area and thereby increase the amount of triboelectric charge generated. When the two friction layer materials are flat structures, the output of Flat PP@Flat NY TENG is the smallest, and the corresponding I_{sc}, V_o, and charge density are 3.0 μA, 62.5 V and 4.4 μC m^{-2}, respectively. When both the friction layer materials are nanostructured, the output of the 200 PP@Nano NY TENG is a maximum, and the corresponding I_{sc}, V_o, and charge density are 16.0 μA, 391 V and 27.6 μC m^{-2}, respectively. Even with the same dual nanostructure, the output of the 400 PP@Nano NY TENG is lower than that of the 200 PP@Nano NY TENG. As can be seen from Fig. S1(a–d),† the number of nanopores per unit area of a polycarbonate filter membrane with a pore size of 200 nm is much greater than that of a polycarbonate filter membrane with a pore size of 400 nm. Therefore, the specific surface area of the prepared 200 PP nanofilm is much larger than that of the 400 PP nanofilm, which results in the 200 PP@Nano NY TENG being able to generate more triboelectric charges and obtain a higher output. In summary, the polypropylene nanowires can effectively increase the output of the triboelectric nanogenerators, and higher-density, relatively smaller-diameter nanowire structure can more effectively increase the output of the triboelectric generators.

The composition of the surface of the friction material is another crucial factor that impacts the performance of a TENG. Normally, for a contact-type triboelectric generator, to increase the output of the triboelectric generator, it is necessary to increase the difference in triboelectric polarity of the two friction layer materials as much as possible. It has been demonstrated that fluoropolymers, such as polytetrafluoroethylene (PTFE) and polyvinylidene fluoride (PVDF), are currently among the most appropriate choices as triboelectric negative friction materials for a TENG. This is primarily because fluorine is the most electronegative element among all the elements. To achieve this, we have implemented a surface chemical modification technique to fine-tune the surface composition of the friction material for a TENG. Here, since PFTS has been proven to have very high triboelectric negative polarity, PFTS was chosen as a modifier to chemically modify the polypropylene film surface. Fig. 5a shows the entire process of physical vapor deposition for depositing and assembling PFTS on the surface of the polypropylene film. Specific experimental steps can be found in the Experimental section. Compared with the surface morphology SEM image before surface modification in Fig. 3b and e, the assembly of PFTS has little effect on the surface morphology of planar and nanostructured films, as shown in Fig. 5b–d. To facilitate data comparison, we abbreviate the above three PFTS modified PP films to flat FPP, 400 FPP and 200 FPP, respectively. To prove that PFTS has been successfully assembled on the surface of the flat PP and PP films with nanostructure, XPS was used to analyze the surface composition of PFTS-modified materials. According to Fig. 5e, there is no F1s characteristic peak in the flat PP film or PP film with nanostructure before PFTS modification. After the physical vapor deposition process, obvious F1s characteristic peaks were detected on the surfaces of flat FPP, 400 FPP and 200 FPP, proving that PFTS had been successfully assembled. In addition, the C1s peak transformed into two peaks, –CF_3 and C–C, after chemical modification, which proved that PFTS had been successfully assembled on the surface of the PP film. In addition, EDS was used to conduct surface element analysis on three chemically modified polypropylene films. As shown in Fig. S3,† EDS surface scanning results show that the F element is distributed very evenly on the surface of the polypropylene films, which also proves that PFTS had been successfully assembled on the surface of the PP films. The water contact angle measurement was also used to verify functionalized PP surfaces. As shown in Fig. S4,† when a water droplet dropped on the flat PP surface, a small contact angle of about 87.9° was observed. After fabrication of 400 nm PP nanowire and 200 nm PP nanowire, water contact angles increased to 145.9° and 145.3°, indicating that the nanostructure is an important factor in creating a hydrophobic or super-hydrophobic surface. After assembling PFTS, the water

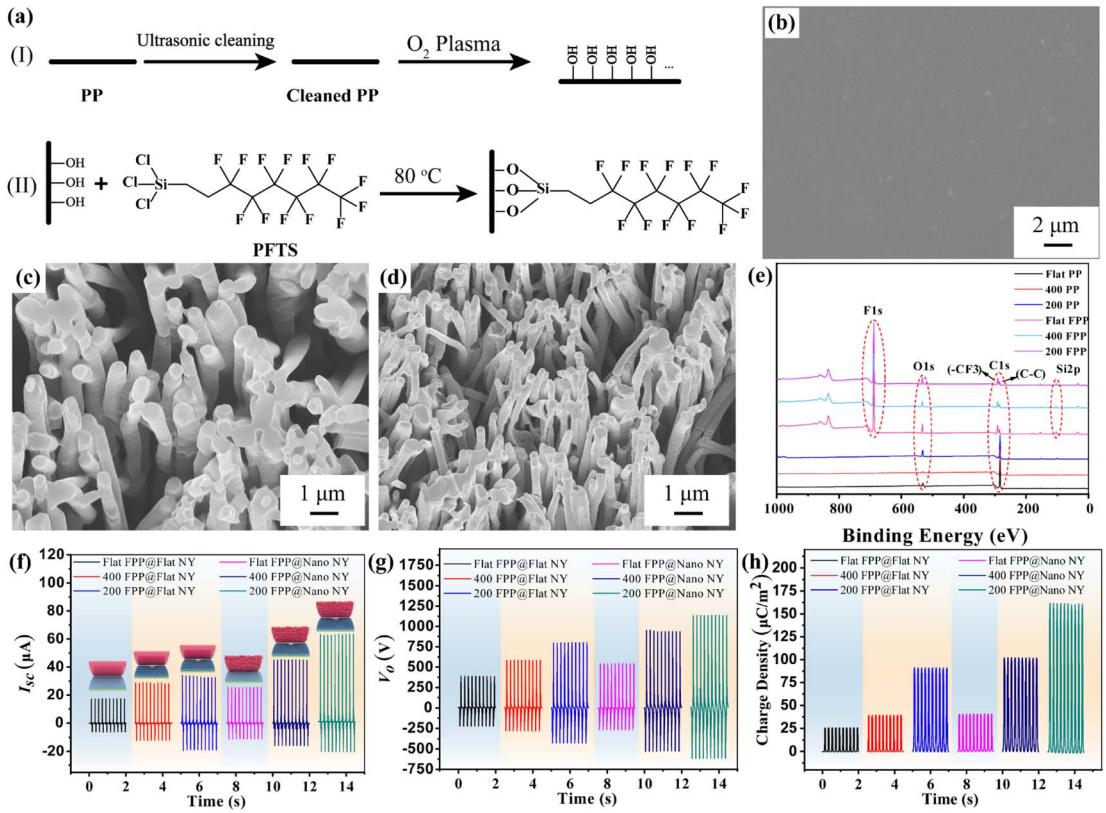

Fig. 5 (a) Schematic diagram of the process of assembling PFTS on the PP surface; surface morphology SEM images of PFTS-modified: (b) flat PP, (c) 400 PP, and (d) 200 PP; (e) XPS spectra of the PP friction layer before and after PFTS modification; output performances of TENGs composed of flat FPP, 400 FPP, 200 FPP, flat NY and NY nanofibers: (f) I_{sc}, (g) V_o and (h) charge density.

contact angles of flat PP, 400 PP and 200 PP were further increased to 111.7°, 153.2°, and 152.2°, respectively. This is mainly due to the fact that the non-polar ($-CF_3$) end groups in PFTS reduce the surface energy of PP and thereby increase its water contact angle.

Like unmodified PP films, a total of six groups of the triboelectric nanogenerators are composed according to different friction layer materials. The short-circuit current, output voltage and charge density results are shown in Fig. 5f–h. Among the six TENGs, the outputs of Flat FPP@Flat NY, 400 FPP@Flat NY, and 200 FPP@Flat NY show a gradually increasing trend, which is the same as that without fluorination modification. Similarly, the outputs of flat FPP@Nano NY, 400 FPP@Nano NY, and 200 FPP@Nano NY show a gradually increasing trend, which is the same as the trend without PFTS modification. However, unlike the output without PFTS modification, the output of the 200 FPP@Flat NY TENG is higher than that of the flat FPP@Nano NY TENG. According to the frictional electrification sequence of the material, the ability of PFTS to be negatively charged during friction is much greater than that of PP, while nylon is very easily positively charged during friction. When the PP film is not modified with PFTS, the ability of polypropylene to generate triboelectric charges cannot be greatly improved simply by nano-treatment of the polypropylene surface. Since NY has a very strong triboelectrically charged ability, the output of a TENG can be improved more by nano-processing NY than by nano-processing polypropylene. Therefore, without fluorination, the output of the 200 PP@Flat NY TENG is smaller than that of the flat PP@Nano NY TENG. When PP is fluorinated, PFTS plays a leading role in improving the output of the TENG, which results in the output of the 200 FPP@Flat NY TENG being higher than that of the Flat FPP@Nano NY TENG. Compared with the output of the planar structure TENG without fluoropolymer modification, after PFTS modification and nano-processing of the nylon material, I_{sc} increased from 3.0 μA to 63.3 μA, V_o increased from 62.5 V to 1135 V and charge density increased from 4.4 μC m^{-2} to 161.5 μC m^{-2}. I_{sc} and V_o increased by more than 18 times, while charge density was increased by about 36 times. It can be seen from the above results that modifying PFTS can greatly increase the amount of tribocharges generated by the triboelectric generator, and PFTS plays a dominant role in improving the output performance of the TENG.

To prove that PFTS significantly promotes the output of the TENG, the surface potentials of the PP, PFTS-PP and NY films were tested using KPFM. In Fig. 6a, b, d and e, it can be seen that the surface potentials of PFTS-PP and PP are negative, and the absolute value of the surface potential of PFTS-PP is significantly improved compared to that of PP. The mean potential value decreased from −12.4 V (PP) to −72.9 V (PFTS-PP), proving that the electron-gathering ability of the PFTS-modified PP film is increased nearly 6 times. Fig. 6c and f

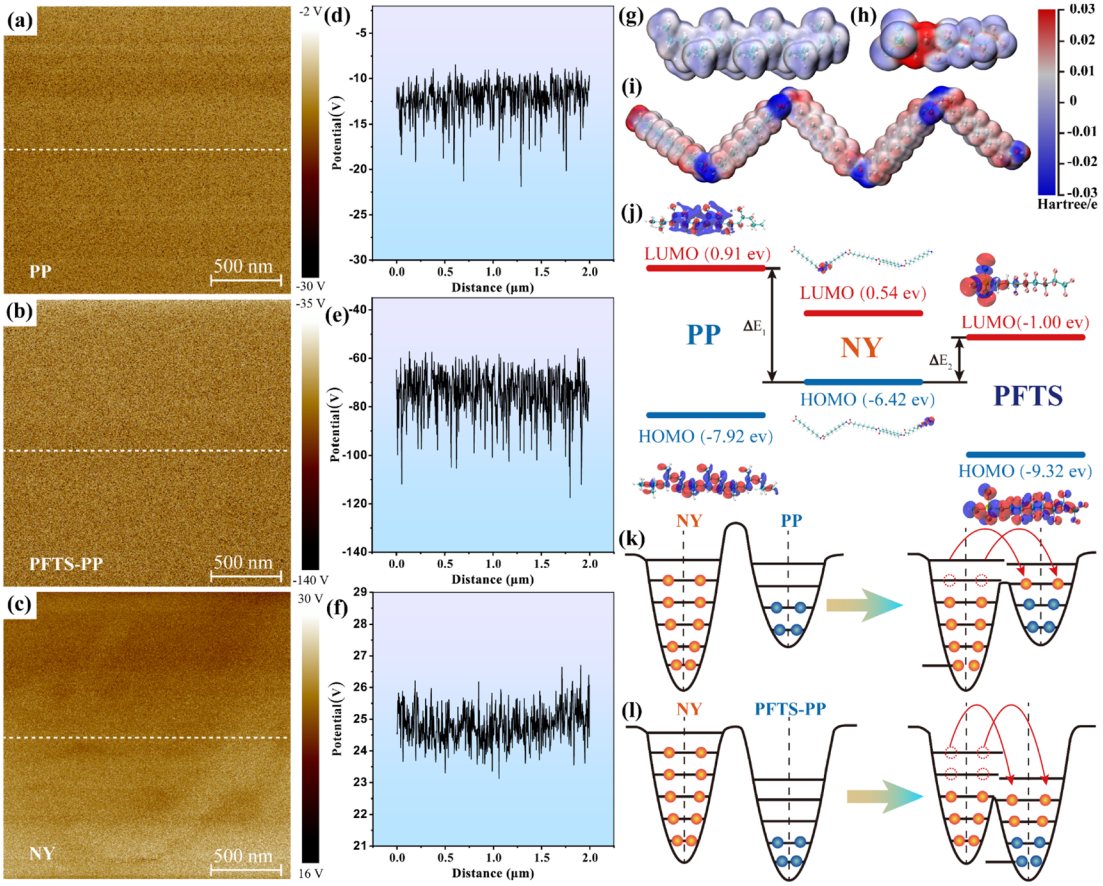

Fig. 6 Surface potential map of (a) PP, (b) PFTS-PP and (c) NY; surface potential line curves of (d) PP, (e) PFTS-PP and (f) NY; calculated ESP maps of (g) PP, (h) PFTS and (i) NY; (j) calculated HOMO and LUMO of PP, PFTS and NY; overlapped electron cloud and potential well model of (k) NY *vs.* PP (l) NY *vs.* PFTS.

show the KPFM results of the NY film. The mean surface potential value of nylon 11 is 25.0 V, which proves that the electron-losing ability of nylon is stronger than the electron-gaining ability of PP and weaker than the electron-gaining ability of PFTS-PP. The calculated electrostatic surface potential (ESP) maps in Fig. 6g–i also prove that PFTS has a more negative potential than PP and nylon has a more positive potential. The output performance of a TENG is proportional to the surface charge density, which essentially depends on the charge transfer capability driven by contact electrification. Previous studies have reported that triboelectric positive materials lose electrons from the HOMO, while triboelectric negative materials gain these electrons from the LUMO.[47,48] Therefore, reducing the energy difference between the HOMO and LUMO of the two friction layer materials can effectively enhance the output of the triboelectric generator. According to the calculated HOMO and LUMO energy and diagrams in Fig. 6j and S5,† the energy difference between the LUMO of PP and HOMO of NY ($\Delta E_1 = 7.33$ eV) is larger than the energy difference between the LUMO of PFTS and HOMO of NY ($\Delta E_2 = 5.42$ eV). According to energy potential well models in Fig. 6k and l, when PP and PFTS are in contact with and separated from nylon, respectively, electrons are more easily transferred from the HOMO of nylon to the LUMO of PFTS, resulting in higher output performance.[49–51] Therefore, it has been experimentally and theoretically proven that self-assembled PFTS can effectively improve the output of polypropylene-based triboelectric nanogenerators.

From the above study, it can be concluded that the 200 FPP@Nano NY TENG with a dual nanowire structure obtained the highest output, and its corresponding I_{sc}, V_o, and charge density are 63.3 μA, 1135 V, 161.5 μC m^{-2}, respectively. The transferred charge density can more intuitively reflect the ability of the friction layer of the triboelectric generator to generate tribocharges. Compared with relevant research results in recent years that use structural design and surface chemical modification to improve the output of contact-separation mode triboelectric nanogenerators, it was found that by combining the design of double nanostructures and chemical modification methods, the charge density obtained in this work can achieve a relatively higher value, as shown in Fig. 7a and Table S1.†,[43,52–56] As an energy conversion device, stability during operation is crucial for practical application. Herein, a durability test was also conducted under 5 Hz contact frequency for the 200 FPP@Nano NY TENG, and the results are shown in Fig. 7b. It can be seen from the test results that the output did

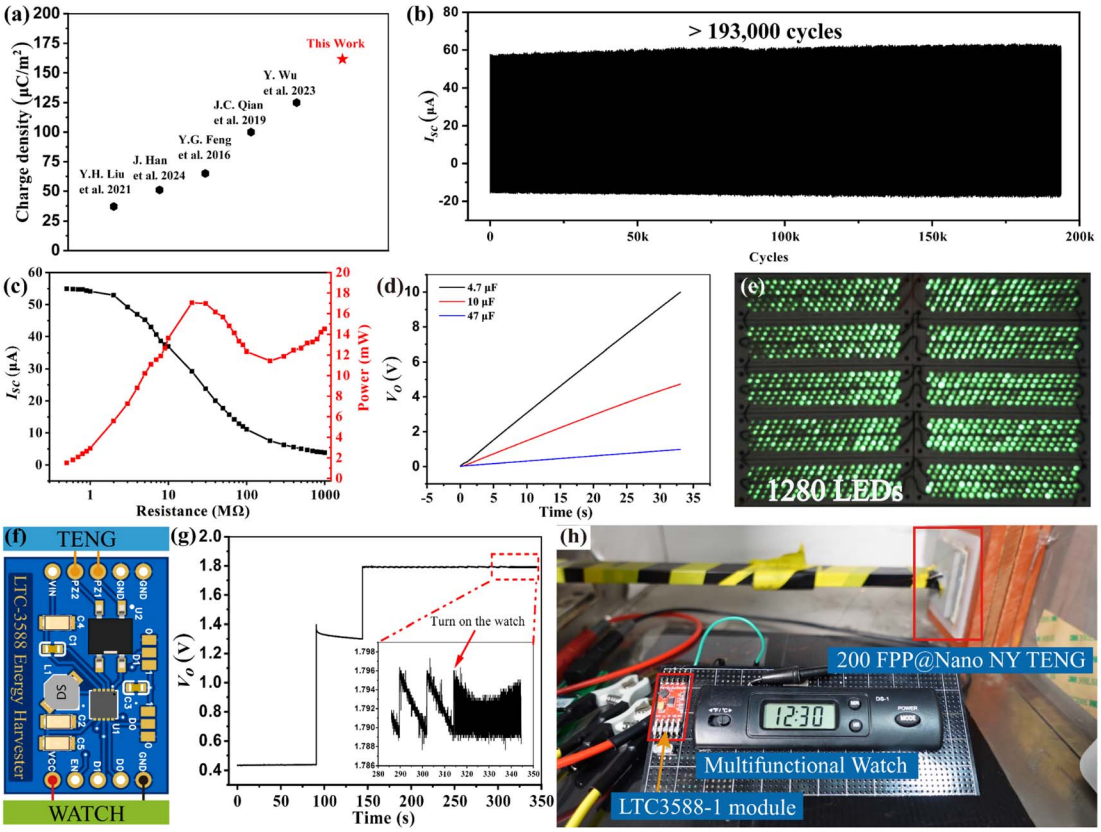

Fig. 7 (a) Comparison of the charge density of CS-TENGs enhanced through structural design and surface modification; (b) long-term stability test of the 200 FPP@Nano NY TENG; (c) I_{sc} and power of the 200 FPP@Nano NY TENG under different load resistances; (d) charging test voltage curves of different capacitors with the 200 FPP@Nano NY TENG as the power supply; (e) photograph of 1280 LEDs connected to the 200 FPP@Nano NY TENG; (f) circuit connection diagram of an LTC3588-1 module as an energy transform device for 200 FPP TENG; (g) the output voltage curve of the LTC3588-1 module before and after turning on the watch; and (h) photograph of the 200 FPP@Nano NY TENG as a power supply for a multifunctional watch.

not decrease during the entire 193 000 cycles of 200 FPP@Nano NY TENG operation, proving that the 200 FPP@Nano NY TENG can maintain a stable output for a long time in practical applications. The output performance of the 200 FPP@Nano NY TENG under different humidities was also tested *via* a sealed acrylic box, as shown in Fig. S6.† As shown in Fig. S7a and S7b,† the output of the TENG shows a decreasing trend as the humidity increases. To more intuitively reflect the changing trend in output with humidity, the relationship between the maximum value of the output and humidity is constructed into a curve, as shown in Fig. S7c and S7d.† As can be seen from Fig. S7c,† as the humidity increases, the maximum value of I_{sc} shows an almost linear decreasing trend with the increase in humidity. The decrease in I_{sc} is relatively slow when the humidity is below 50%, and the rate of decrease increases significantly when the humidity is over 50%. This trend looks more obvious with V_o. Overall, the 200 FPP@Nano NY TENG, like most TENGs, does not have anti-humidity characteristics. However, it can maintain a relatively high output with an output of 52.8 μA and 1076 V when used in an environment with humidity below 50%. Fig. 7c shows the I_{sc} values of the 200 FPP@Nano NY TENG under different load resistances from 0.1 MΩ to 1000 MΩ, and its corresponding power. According to the test results, current decreases with the increase in loading resistance, while the calculated output power of the device first rises and later drops with increasing resistance. The maximum value of the output power is about 17.0 mW under a loading resistance of 20 MΩ. As a power supply, the 200 FPP@Nano NY TENG has also been rectified for charging capacitors with different capacities. As shown in Fig. 7d, it took the 200 FPP@Nano NY TENG 33 s to charge 4.7 μF, 10 μF and 47 μF capacitors to 10 V, 4.7 V and 1.0 V, respectively. Furthermore, to verify that the generated electricity can indeed be used as an energy supply, the 200 FPP@Nano NY TENG was rectified to power 1280 LEDs. As shown in Fig. 7e and Video S1,† driven by a linear motor, the 200 FPP@Nano NY TENG can instantly light up 1280 commercial LEDs. Besides, the AC current generated by the 200 FPP@Nano NY TENG can be converted to DC current *via* an LTC3588-1 module and stored in integrated capacitors as a power supply for a multifunctional electronic watch. Fig. 7f shows the circuit connection diagram of the LTC3588-1 module, TENG and a multi-functional electronic watch. According to Fig. 7g, when the TENG runs for about 150 s, the output voltage of the LTC3588-1 module stabilizes at 1.8 V. To ensure that the electronic watch can run for a long time, it should continue to run for a period of time to charge the capacitor on the module,

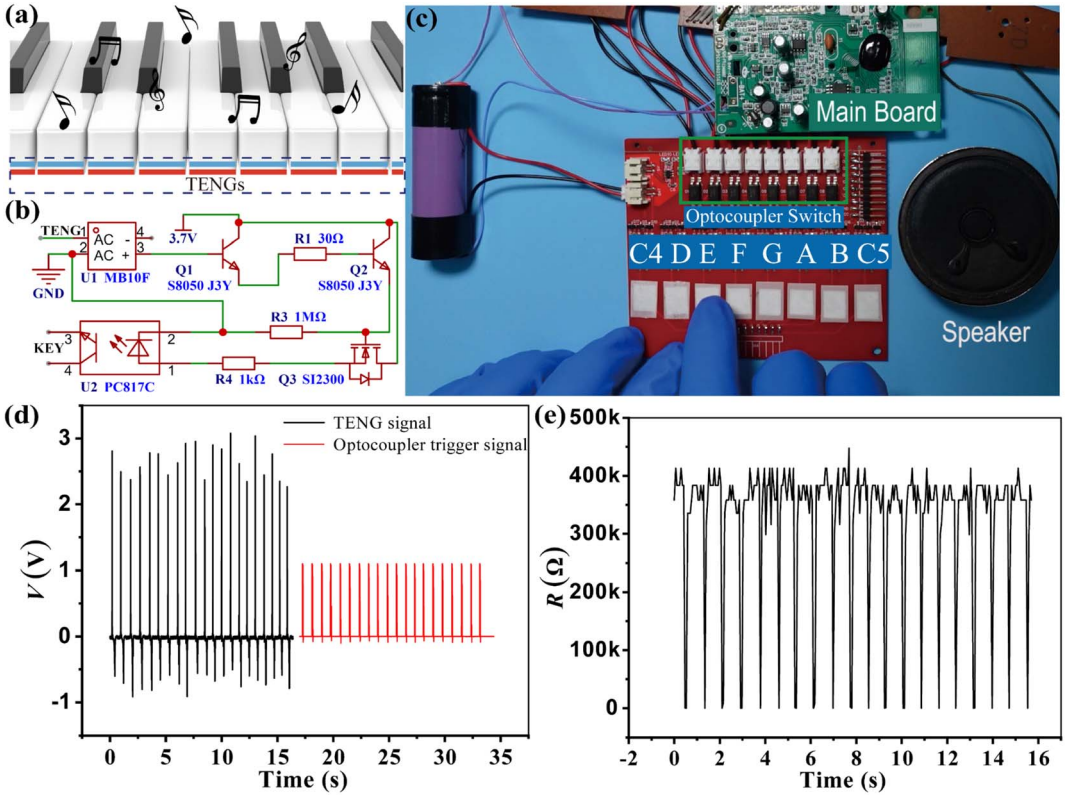

Fig. 8 (a) Schematic image of the 200 FPP TENG as a trigger signal for controlling an optocoupler switch; (b) PCB schematic diagram of a TENG triggering an optocoupler switch; (c) photograph of the 200 FPP TENG as a trigger signal for controlling an optocoupler switch; (d) comparison of the TENG and trigger signals when the optocoupler switch is triggered; and (e) changes in the resistance of the photocoupler terminal when the optocoupler switch is triggered.

and the electronic power should not be turned off before 300 s. It can also be seen that the voltage curve can remain stable without a sufficient power supply. As shown in Fig. 7h and Video S2,† after 5 minutes of charging, the LTC3588-1 module can continuously supply power to a multi-functional electronic watch with a temperature measurement function and ensure the normal operation of the electronic watch. This also proves that the 200 FPP@Nano NY TENG can be used for energy storage and to power small electronic devices for a long time.

In view of the long-term durability and high frictional electrification performance of the 200 FPP film, it was integrated into an PCB circuit to control the 'on' and 'off' of an optocoupler switch. Fig. 8a and b show schematic images of the 200 FPP TENG as a trigger signal for controlling an optocoupler switch and PCB schematic diagram of the TENG triggering an optocoupler switch. As shown in Fig. 8c and Video S3†, eight 200 FPP films were pasted on the PCB using double-sided conductive tape to form a single-electrode TENG, which was used to generate pulse signals that excited the optocoupler switch. Each TENG was used to control a key of an electronic piano from C4 to C5. When a finger touches the FPP film, the triboelectric signal generated can activate the corresponding optocoupler switch and emit the corresponding key sound. By pressing different TENGs, a complete piece of music can be played. It can be seen from Fig. 8d that after processing, the TENG signal changes from an AC signal to a more regular trigger signal. When the optocoupler switch is triggered, the resistance at the load end also changes from 400 kΩ to 0 Ω in Fig. 8e, which proves that the TENG signal can normally turn on the optocoupler switch. Therefore, the 200 FPP@Nano NY TENG with a PFTS-modified double nanowire structure prepared by a simple method has very high output performance and great application prospects in practical use.

Conclusions

PP nanowires and electrospun nylon nanofibers were successfully prepared through a simple and time-saving method with a high success rate. The polypropylene nanowire film and nylon nanofiber film were assembled into a dual nanostructure TENG to enhance its output performance. Furthermore, PFTS was assembled on the surface of the polypropylene film using a vapor deposition method to further enhance the output of the TENG. Among the 12 TENGs in this study, the 200 FPP@Nano NY TENG obtained the maximum I_{sc}, V_o, and charge density of 63.3 μA, 1135 V, 161.5 μC m^{-2}, respectively. Compared with a planar structure TENG, I_{sc} and V_o were increased by about 18 times, while the charge density was increased by about 36 times. In addition, the TENG showed no reduction in output after continuous operation for more than 193 000 cycles, demonstrating very good working stability for practical use. The maximum value of output power of the 200 FPP@Nano NY

TENG is about 17.0 mW under a loading resistance of 20 MΩ. The electricity generated by this TENG can successfully light up 1280 LEDs and continuously supply power to a multi-functional electronic watch, proving that it has very good application prospects in micro power supply devices. Finally, the 200 FPP TENG was integrated into a PCB circuit to control the 'on' and 'off' of an optocoupler switch, indicating application prospects in remote control switching circuits.

Data availability

All data have been presented in the manuscript and ESI.†

Author contributions

Yanhong Dong: conceptualization, methodology, validation, investigation, writing – original draft. Yange Feng: conceptualization, investigation, software, funding acquisition, writing – review & editing. Daoai Wang: conceptualization, resources, writing – review & editing, supervision, project administration, funding acquisition.

Conflicts of interest

The authors declare that they have no known competing financial interests or personal relationships that could have appeared to influence the work reported in this paper.

Acknowledgements

We thank the Strategic Priority Research Program of the Chinese Academy of Sciences (Grant No. XDB0470103), National Natural Science Foundation of China (Grant No. 52275219 and U21A2046), Program for Taishan Scholars of Shandong Province (No. ts20190965), Western Light Project of CAS (xbzg-zdsys-202118), Major Science and Technology Projects in Gansu Province (No. 22ZD6GA002), Key Research and Development Program in Shandong Province (No. SYS202203) and Major Program of the Lanzhou Institute of Chemical Physics, CAS (No. ZYFZFX-5) for the financial support.

References

1 F.-R. Fan, Z.-Q. Tian and Z. L. Wang, Flexible triboelectric generator, *Nano Energy*, 2012, **1**, 328–334.
2 Z. L. Wang, Triboelectric Nanogenerators as New Energy Technology for Self-Powered Systems and as Active Mechanical and Chemical Sensors, *ACS Nano*, 2013, **7**, 9533–9557.
3 L. Zhou, D. Liu, L. Liu, L. He, X. Cao, J. Wang and Z. L. Wang, Recent Advances in Self-Powered Electrochemical Systems, *Research*, 2021, 1–15.
4 Y.-C. Lai, J. Deng, S. Niu, W. Peng, C. Wu, R. Liu, Z. Wen and Z. L. Wang, Electric Eel-Skin-Inspired Mechanically Durable and Super-Stretchable Nanogenerator for Deformable Power Source and Fully Autonomous Conformable Electronic-Skin Applications, *Adv. Mater.*, 2016, **28**, 10024–10032.
5 S. K. Ghosh, P. Adhikary, S. Jana, A. Biswas, V. Sencadas, S. D. Gupta, B. Tudu and D. Mandal, Electrospun gelatin nanofiber based self-powered bio- e -skin for health care monitoring, *Nano Energy*, 2017, **36**, 166–175.
6 M. Xu, Y.-C. Wang, S. L. Zhang, W. Ding, J. Cheng, X. He, P. Zhang, Z. Wang, X. Pan and Z. L. Wang, An aeroelastic flutter based triboelectric nanogenerator as a self-powered active wind speed sensor in harsh environment, *Extreme Mech. Lett.*, 2017, **15**, 122–129.
7 L. Fang, Q. Zheng, W. Hou, J. Gu and L. Zheng, A self-powered tilt angle sensor for tall buildings based on the coupling of multiple triboelectric nanogenerator units, *Sens. Actuators, A*, 2023, **349**, 114015.
8 L. He, C. Zhang, B. Zhang, O. Yang, W. Yuan, L. Zhou, Z. Zhao, Z. Wu, J. Wang and Z. L. Wang, A Dual-Mode Triboelectric Nanogenerator for Wind Energy Harvesting and Self-Powered Wind Speed Monitoring, *ACS Nano*, 2022, **16**, 6244–6254.
9 C. Zhang, Y. Liu, B. Zhang, O. Yang, W. Yuan, L. He, X. Wei, J. Wang and Z. L. Wang, Harvesting Wind Energy by a Triboelectric Nanogenerator for an Intelligent High-Speed Train System, *ACS Energy Lett.*, 2021, **6**, 1490–1499.
10 W. Xu, H. Zheng, Y. Liu, X. Zhou, C. Zhang, Y. Song, X. Deng, M. Leung, Z. Yang, R. X. Xu, Z. L. Wang, X. C. Zeng and Z. Wang, A droplet-based electricity generator with high instantaneous power density, *Nature*, 2020, **578**, 392–396.
11 J. Meng, L. Zhang, H. Liu, W. Sun, W. Wang, H. Wang, D. Yang, M. Feng, Y. Feng and D. Wang, A New Single-Electrode Generator for Water Droplet Energy Harvesting with A 3 mA Current Output, *Adv. Energy Mater.*, 2024, **14**, 2303298.
12 J. Zhang, S. Lin and Z. L. Wang, Triboelectric Nanogenerator Array as a Probe for In Situ Dynamic Mapping of Interface Charge Transfer at a Liquid–Solid Contacting, *ACS Nano*, 2023, **17**, 1646–1652.
13 X. Pu, C. Zhang and Z. L. Wang, Triboelectric nanogenerators as wearable power sources and self-powered sensors, *Natl. Sci. Rev.*, 2023, **10**, nwac170.
14 W. Yan, Y. Liu, P. Chen, L. N. Y. Cao, J. An, T. Jiang, W. Tang, B. Chen and Z. L. Wang, Flexible Film-Discharge-Switch Assisted Universal Power Management System for the Four Operation Modes of Triboelectric Nanogenerators, *Adv. Energy Mater.*, 2022, **12**, 2103677.
15 K.-B. Chang, P. Parashar, L.-C. Shen, A.-R. Chen, Y.-T. Huang, A. Pal, K.-C. Lim, P.-H. Wei, F.-C. Kao, J.-J. Hu and Z.-H. Lin, A triboelectric nanogenerator-based tactile sensor array system for monitoring pressure distribution inside prosthetic limb, *Nano Energy*, 2023, **111**, 108397.
16 H. Lei, Y. Chen, Z. Gao, Z. Wen and X. Sun, Advances in self-powered triboelectric pressure sensors, *J. Mater. Chem. A*, 2021, **9**, 20100–20130.
17 G. Lee, S. Lee, D. Kim, S. H. Kim, C. Choi, S. G. Lee and K. Cho, Anisotropic Fluorinated-Elastomer-Blended Micro-Dominoes for Wearable Triboelectric Nanogenerators, *Adv. Funct. Mater.*, 2024, 2316288.
18 J. Shen, B. Li, Y. Yang, Z. Yang, X. Liu, K. C. Lim, J. Chen, L. Ji, Z. H. Lin and J. Cheng, Application, challenge and

perspective of triboelectric nanogenerator as micro-nano energy and self-powered biosystem, *Biosens. Bioelectron.*, 2022, **216**, 114595.

19 C. Cao, Z. Li, F. Shen, Q. Zhang, Y. Gong, H. Guo, Y. Peng and Z. L. Wang, Progress in techniques for improving the output performance of triboelectric nanogenerators, *Energy Environ. Sci.*, 2024, **17**, 885–924.

20 Q. Zhang, T. Jin, J. Cai, L. Xu, T. He, T. Wang, Y. Tian, L. Li, Y. Peng and C. Lee, Wearable Triboelectric Sensors Enabled Gait Analysis and Waist Motion Capture for IoT-Based Smart Healthcare Applications, *Adv. Sci.*, 2022, **9**, e2103694.

21 F. Yi, Z. Zhang, Z. Kang, Q. Liao and Y. Zhang, Recent Advances in Triboelectric Nanogenerator-Based Health Monitoring, *Adv. Funct. Mater.*, 2019, **29**, 1808849.

22 D. Yang, Y. Ni, X. Kong, S. Li, X. Chen, L. Zhang and Z. L. Wang, Self-Healing and Elastic Triboelectric Nanogenerators for Muscle Motion Monitoring and Photothermal Treatment, *ACS Nano*, 2021, **15**, 14653–14661.

23 C. Yeh, F.-C. Kao, P.-H. Wei, A. Pal, K. Kaswan, Y.-T. Huang, P. Parashar, H.-Y. Yeh, T.-W. Wang, N. Tiwari, T.-T. Tsai, Y.-F. Huang and Z.-H. Lin, Bioinspired shark skin-based liquid metal triboelectric nanogenerator for self-powered gait analysis and long-term rehabilitation monitoring, *Nano Energy*, 2022, **104**, 107852.

24 M.-Z. Huang, P. Parashar, A.-R. Chen, S.-C. Shi, Y.-H. Tseng, K. C. Lim, H.-Y. Yeh, A. Pal, D.-Y. Kang and Z.-H. Lin, Snake-scale stimulated robust biomimetic composite triboelectric layer for energy harvesting and smart health monitoring, *Nano Energy*, 2024, **122**, 109266.

25 H. Chen, C. Xing, Y. Li, J. Wang and Y. Xu, Triboelectric nanogenerators for a macro-scale blue energy harvesting and self-powered marine environmental monitoring system, *Sustainable Energy Fuels*, 2020, **4**, 1063–1077.

26 S. Sardana, Z. Singh, A. K. Sharma, N. Kaur, P. K. Pati and A. Mahajan, Self-powered biocompatible humidity sensor based on an electrospun anisotropic triboelectric nanogenerator for non-invasive diagnostic applications, *Sens. Actuators, B*, 2022, **371**, 132507.

27 Q. Zhang, C. Jiang, X. Li, S. Dai, Y. Ying and J. Ping, Highly Efficient Raindrop Energy-Based Triboelectric Nanogenerator for Self-Powered Intelligent Greenhouse, *ACS Nano*, 2021, **15**, 12314–12323.

28 S. Shen, J. Fu, J. Yi, L. Ma, F. Sheng, C. Li, T. Wang, C. Ning, H. Wang, K. Dong and Z. L. Wang, High-Efficiency Wastewater Purification System Based on Coupled Photoelectric-Catalytic Action Provided by Triboelectric Nanogenerator, *Nano-Micro Lett.*, 2021, **13**, 194.

29 C.-L. Li, W.-Z. Song, D.-J. Sun, M. Zhang, J. Zhang, Y.-Q. Chen, S. Ramakrishna and Y.-Z. Long, A self-priming air filtration system based on triboelectric nanogenerator for active air purification, *Chem. Eng. J.*, 2023, **452**, 139428.

30 L.-B. Huang, W. Xu, W. Tian, J.-C. Han, C.-H. Zhao, H.-L. Wu and J. Hao, Ultrasonic-assisted ultrafast fabrication of polymer nanowires for high performance triboelectric nanogenerators, *Nano Energy*, 2020, **71**, 104593.

31 Y. Liu, R. Han, L. Li, Z. Zhou, G. Chen and Q. Li, Tuning of Highly Dielectric Calcium Copper Titanate Nanowires To Enhance the Output Performance of a Triboelectric Nanogenerator, *ACS Appl. Electron. Mater.*, 2020, **2**, 1709–1715.

32 Y. Zhong, J. Wang, L. Han, S. Dai, H. Zhu, J. Hua, G. Cheng and J. Ding, High-performance flexible self-powered triboelectric pressure sensor based on chemically modified micropatterned PDMS film, *Sens. Actuators, A*, 2023, **349**, 114013.

33 V. A. Cao, M. Kim, S. Lee, P. C. Van, J.-R. Jeong, P. Park and J. Nah, Chemically modified MXene nanoflakes for enhancing the output performance of triboelectric nanogenerators, *Nano Energy*, 2023, **107**, 108128.

34 C.-C. Wang and C.-Y. Chang, Enhanced output performance and stability of triboelectric nanogenerators by employing silane-based self-assembled monolayers, *J. Mater. Chem. C*, 2020, **8**, 4542–4548.

35 T. I. Kim, I. J. Park, S. Kang, T. S. Kim and S. Y. Choi, Enhanced Triboelectric Nanogenerator Based on Tungsten Disulfide via Thiolated Ligand Conjugation, *ACS Appl. Mater. Interfaces*, 2021, **13**, 21299–21309.

36 Y. Liu, J. Mo, Q. Fu, Y. Lu, N. Zhang, S. Wang and S. Nie, Enhancement of Triboelectric Charge Density by Chemical Functionalization, *Adv. Funct. Mater.*, 2020, **30**, 2004714.

37 S. A. Lone, K. C. Lim, K. Kaswan, S. Chatterjee, K.-P. Fan, D. Choi, S. Lee, H. Zhang, J. Cheng and Z.-H. Lin, Recent advancements for improving the performance of triboelectric nanogenerator devices, *Nano Energy*, 2022, **99**, 107318.

38 X. Cheng, B. Meng, X. Chen, M. Han, H. Chen, Z. Su, M. Shi and H. Zhang, Single-Step Fluorocarbon Plasma Treatment-Induced Wrinkle Structure for High-Performance Triboelectric Nanogenerator, *Small*, 2016, **12**, 229–236.

39 X. Fan, J. Chen, J. Yang, P. Bai, Z. Li and Z. L. Wang, Ultrathin, rollable, paper-based triboelectric nanogenerator for acoustic energy harvesting and self-powered sound recording, *ACS Nano*, 2015, **9**, 4236–4243.

40 L. Lin, S. Wang, S. Niu, C. Liu, Y. Xie and Z. L. Wang, Noncontact free-rotating disk triboelectric nanogenerator as a sustainable energy harvester and self-powered mechanical sensor, *ACS Appl. Mater. Interfaces*, 2014, **6**, 3031–3038.

41 Z.-H. Lin, Y. Xie, Y. Yang, S. Wang, G. Zhu and Z. L. Wang, Enhanced Triboelectric Nanogenerators and Triboelectric Nanosensor Using Chemically Modified TiO2 Nanomaterials, *ACS Nano*, 2013, **7**, 4554–4560.

42 D. Choi, Y. Lee, Z. H. Lin, S. Cho, M. Kim, C. K. Ao, S. Soh, C. Sohn, C. K. Jeong, J. Lee, M. Lee, S. Lee, J. Ryu, P. Parashar, Y. Cho, J. Ahn, I. D. Kim, F. Jiang, P. S. Lee, G. Khandelwal, S. J. Kim, H. S. Kim, H. C. Song, M. Kim, J. Nah, W. Kim, H. G. Menge, Y. T. Park, W. Xu, J. Hao, H. Park, J. H. Lee, D. M. Lee, S. W. Kim, J. Y. Park, H. Zhang, Y. Zi, R. Guo, J. Cheng, Z. Yang, Y. Xie, S. Lee, J. Chung, I. K. Oh, J. S. Kim, T. Cheng, Q. Gao, G. Cheng, G. Gu, M. Shim, J. Jung, C. Yun, C. Zhang, G. Liu, Y. Chen, S. Kim, X. Chen, J. Hu, X. Pu, Z. H. Guo, X. Wang, J. Chen, X. Xiao, X. Xie, M. Jarin, H. Zhang, Y. C. Lai, T. He, H. Kim, I. Park, J. Ahn, N. D. Huynh, Y. Yang, Z. L. Wang,

J. M. Baik and D. Choi, Recent Advances in Triboelectric Nanogenerators: From Technological Progress to Commercial Applications, *ACS Nano*, 2023, **17**, 11087–11219.

43 Y. Feng, Y. Zheng, S. Ma, D. Wang, F. Zhou and W. Liu, High output polypropylene nanowire array triboelectric nanogenerator through surface structural control and chemical modification, *Nano Energy*, 2016, **19**, 48–57.

44 T. Lu and F. Chen, Multiwfn: a multifunctional wavefunction analyzer, *J. Comput. Chem.*, 2012, **33**, 580–592.

45 J. Zhang and T. Lu, Efficient evaluation of electrostatic potential with computerized optimized code, *Phys. Chem. Chem. Phys.*, 2021, **23**, 20323–20328.

46 W. Humphrey, A. Dalke and K. Schulten, VMD: Visual molecular dynamics, *J. Mol. Graphics*, 1996, **14**, 33–38.

47 J. Wu, X. Wang, H. Li, F. Wang and Y. Hu, First-principles investigations on the contact electrification mechanism between metal and amorphous polymers for triboelectric nanogenerators, *Nano Energy*, 2019, **63**, 103864.

48 S. M. Nawaz, M. Chatterjee, S. Chakrabarti, N. Sepay and A. Mallik, Realization of a highly-performing triboelectric nanogenerator utilizing molecular self-assembly, *Nano Energy*, 2023, **117**, 108924.

49 S. Lin, C. Xu, L. Xu and Z. L. Wang, The Overlapped Electron-Cloud Model for Electron Transfer in Contact Electrification, *Adv. Funct. Mater.*, 2020, **30**, 1909724.

50 Z. L. Wang and A. C. Wang, On the origin of contact-electrification, *Mater. Today*, 2019, **30**, 34–51.

51 M. Willatzen and Z. Lin Wang, Theory of contact electrification: Optical transitions in two-level systems, *Nano Energy*, 2018, **52**, 517–523.

52 Y. Wu, X. Wang, Y. Wang, Y. Nan, H. Xu, H. Zhou, M. Ren, J. Duan, Y. Huang and B. Hou, Enhancing the Performance of Triboelectric Nanogenerator Via Facile PDMS Surface Modification, *Adv. Eng. Mater.*, 2023, **25**, 2201442.

53 J. Qian, J. He, S. Qian, J. Zhang, X. Niu, X. Fan, C. Wang, X. Hou, J. Mu, W. Geng and X. Chou, A Nonmetallic Stretchable Nylon-Modified High Performance Triboelectric Nanogenerator for Energy Harvesting, *Adv. Funct. Mater.*, 2019, **30**, 1907414.

54 J. Han, J. Li, X. Zhang, L. Zhao and C. Wang, Enhancing the performance of triboelectric nanogenerator via chitosan films surface modification, *Chem. Eng. J.*, 2024, **489**, 151493.

55 Y. Liu, Q. Fu, J. Mo, Y. Lu, C. Cai, B. Luo and S. Nie, Chemically tailored molecular surface modification of cellulose nanofibrils for manipulating the charge density of triboelectric nanogenerators, *Nano Energy*, 2021, **89**, 106369.

56 J. Zhou, C. Lu, D. Lan, Y. Zhang, Y. Lin, L. Wan, W. Wei, Y. Liang, D. Guo, Y. Liu and W. Yu, Enhancing the Output Performance of a Triboelectric Nanogenerator Based on Modified Polyimide and Sandwich-Structured Nanocomposite Film, *Nanomaterials*, 2023, **13**, 1056.